A Kagome lattice of lanthanide atoms in a 2d er-directed metal-organic coordination network

Daniel Moreno, Sofía O. Parreiras, Shanmugasibi K. Mathialagan, María Tenorio, Koen Lauwaet, José I. Urgel, José M. Gallego* and D. Écija*

A Kagome Lattice of Lanthanide Atoms in a 2D Er-directed Metal-Organic Coordination Network

Daniel Moreno,[a] Sofía O. Parreiras,[a] Shanmugasibi K. Mathialagan,[a] María Tenorio,[a] Koen Lauwaet,[a] José I. Urgel,[a][b] José M. Gallego*[c] and D. Écija*[a][b]

[a] Dr. D. Moreno, Dr. S. O. Parreiras, S. K. Mathialagan, Dr. M. Tenorio, Dr. K. Lauwaet, Dr. J. I. Urgel, Prof. Dr. D. Écija
Instituto Madrileño de Estudios Avanzados en Nanociencia (IMDEA Nanociencia)
C/ Faraday 9. Campus de Cantoblanco, 28049 Madrid, Spain,
E-mail: david.ecija@imdea.org

[b] Dr. J. I. Urgel, Prof. Dr. D. Écija
Unidad de Nanomateriales Avanzados
Instituto Madrileño de Estudios Avanzados en Nanociencia (IMDEA Nanociencia)
Unidad Asociada al CSIC por el ICMM
Campus de Cantoblanco, 28049 Madrid, Spain

[c] Dr. J. M. Gallego
Instituto de Ciencia de Materiales de Madrid (ICMM), CSIC
C/ Sor Juana Inés de la Cruz 3. Campus de Cantoblanco, 28049 Madrid, Spain
E-mail: josemaria.gallego@csic.es

Supporting information for this article is given via a link at the end of the document.

Abstract: Kagome lattices have attracted much attention due the very interesting properties they can exhibit, both from the electronic and the magnetic points of view, although much of the experimental studies have been reported on 3D metals or 2D nanosheets. In the past few years, on-surface synthesis has allowed the fabrication of strictly monolayer 2D metal-organic networks, many of them containing transition metals. In this paper we report the fabrication and the study of the electronic and magnetic properties of a monolayer 2D metal-organic network where the nodes are lanthanide atoms forming a kagome lattice.

Introduction

Ever since the first theoretical studies,[1] kagome lattices have been the subject of a lot of attention due to the fascinating properties arising from magnetic spin frustration.[2,3] A kagome lattice is formed by a network of corner-sharing triangles and hexagons. Here, each atom has four neighboring atoms and is described by the indices (3636), meaning that if we start counting the rings around any vertex from one of the triangles we encounter in order (independent of the direction of motion) a triangle followed by a hexagon, then another triangle and finally another hexagon (Figure 1a). When incorporating magnetic moments, they can display non-collinear spin structures,[4] quantum spin-liquid states,[5] fractionalized spin excitations,[6] ferromagnetic Weyl-semimetallic states,[7] giant anomalous Hall effect,[8] or quantum anomalous Hall effect.[9] But even in the absence of magnetism, the electronic band structure naturally includes Dirac cones, flat bands and van Hove singularities, which can be the origin of different exotic properties, like non-trivial topological states, superconductivity, etc.[10–16]

Strictly speaking, kagome lattices are 2D systems, although most of the experimental studies have been done on 3D crystals, where they can be found forming 2D planes,[17,18] or on quasi-2D nanosheets,[19–21] systems where bulk characterization techniques can be used. Some 3D crystals containing lanthanide elements have been synthesized, either by forming part of the kagome lattice,[22,23] or being intercalated between the kagome planes.[24] The introduction of large magnetic moments, strong spin-orbit coupling and high magnetic anisotropies confer these materials an extra interest.[23,25,26]

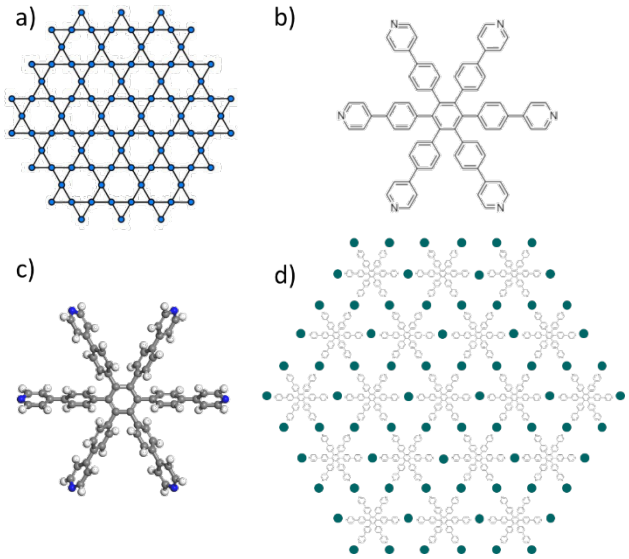

Figure 1: a) Sketch of the structure of a Kagome lattice. b) Schematic structure of the TTDP molecule. d) DFT optimized configuration of TTDP. d) Schematic structure of the TTDP-Er metal-organic network reported in this paper.

On the other hand, molecular self-assembly on solid surfaces and on-surface synthesis have allowed the fabrication of truly 2D monolayer kagome lattices, either all-organic,[27–29] or much more interesting, as metal-organic coordination networks (MOCNs).[30,31] These systems are reticular materials composed of one or more metal ions bonded to surrounding organic linkers,

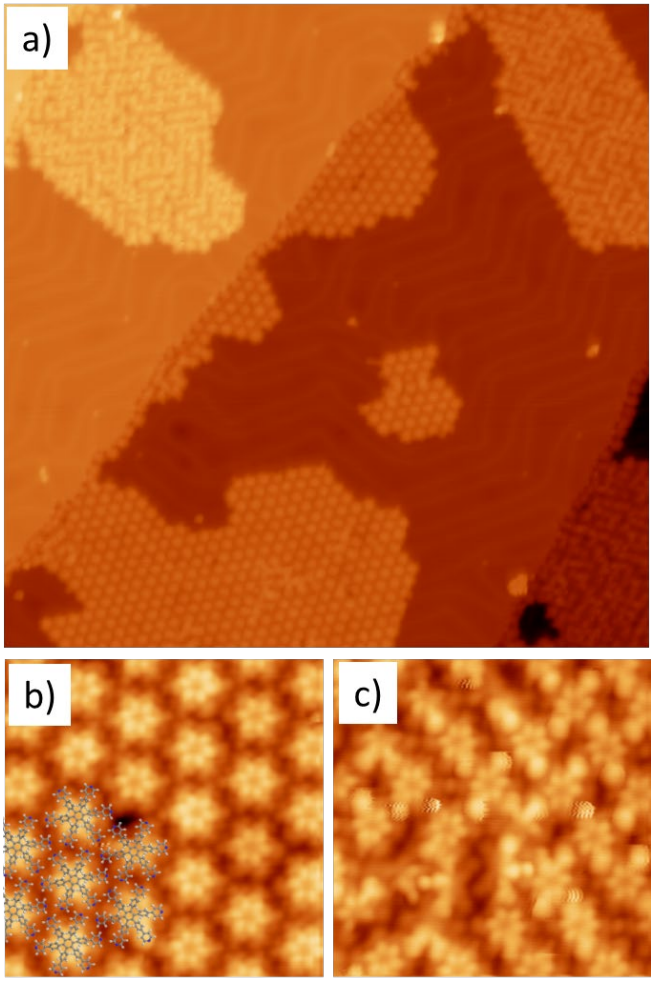

Figure 2: STM images of the Au(111) surface after depositing a submonolayer amount of TTPD with the substrate held at room temperature. *a) 100 nm × 100 nm; 0.5 V, 0.03 nA; b) 10 nm × 10 nm; 0.5 V, 0.02 nA; c) 10 nm × 10 nm; 0.5 V, 0.01 nA.*

and given the huge number of possible metal-organic combinations, on-surface synthesis has allowed the fabrication of many different networks, in terms of topology, crystalline structure, pore shape and size,[32,33] including kagome lattices.[34–41] More recently, lanthanide-containing metal-organic networks have also been reported.[42–48] But, to the best of our knowledge, in the only example where a kagome lattice containing lanthanide elements was reported, the nodes of the lattice were actually binuclear,[47] thus breaking the very first requirement needed for the existence of geometrical magnetic frustration.

In this paper we describe the on-surface synthesis of an Er-directed metal-organic coordination network, prepared by sequential deposition of 4,4'-(3',4',5',6'-Tetrakis(4-(pyridin-4-yl)phenyl)-[1,1':2',1''-terphenyl]-4,4''-diyl)dipyridine (TTDP) (Figure 1b) and Er atoms on Au(111). After annealing to 200 °C, a perfect kagome lattice is formed, with the Er atoms at the nodes of the lattice and the TTDP molecules at the center of the hexagon rings.

Results and Discussion

TTDP has hexagonal symmetry, with six carbon rings connected to a central carbon ring through single, rotatable bonds, and six additional pyridyl groups connected to the first ones in a star-like way (Figure 1b). While the central carbon ring is parallel to the main molecular plane, steric hindrance induces the remaining carbon rings to rotate with respect to this plane, with all the rings in the middle circle rotated in the same direction and all the pyridyl groups rotated in the opposite direction (Figure 1c). DFT calculations indicate that the N atoms are negatively charged (-0.3 $|e^-|$), while the HOMO-LUMO separation gap is ~ 3.15 eV.

Figure 2a shows an overview of the Au(111) surface after depositing a submonolayer amount of TTDP (~0.3 ML) with the substrate held at room temperature. The STM images show that there are two different types of islands on the surface. In the first one, Figure 2b, all the molecules look very similar, apparently with the main plane parallel to the surface (although the middle circle looks brighter than the outer one), forming a hexagonal network with a lattice parameter of 20.9 ± 0.5 Å. The STM data are compatible with a lattice with an epitaxial relationship with the Au substrate described by the matrix

$$\begin{pmatrix} 8 & 4 \\ -4 & 4 \end{pmatrix},$$

which has a lattice parameter of 20.0 Å. Scanning tunneling spectroscopy (see Figure S1), shows that the organic layer has two strong resonances at -2.4 eV and 2.3 eV (LUMO), plus a smaller one at -1.6 eV (HOMO), which would give a band gap of ~3.9 eV.

Figure S2 shows the results of DFT calculations of the optimized adsorption geometry of one monolayer of TTDP on Au(111) following the experimental structure. As suggested by the STM images, the molecules lie almost flat on the surface. The rings in the outer circle are the closest to the surface, while the central ring is the one furthest from the surface. Steric hindrance between the H atoms in the benzene rings makes the middle rings to rotate away from being parallel to the surface, which makes them to be the brightest in the STM images. The self-assembly geometry seems to be driven by H bonds between the terminal N atoms and the H atoms of nearby molecules. The projected density of states reflects a band gap of 2.94 eV, which is only slightly smaller than the calculated for a free-standing layer with the adsorption geometry (2.96 eV), indicating a relatively weak interaction with the substrate. On the other hand, the band gap of a free-standing layer in the relaxed geometry is 3.15 eV.

In the second type of islands the arrangement is much more irregular, with some much brighter lobes per molecule, and molecular centers separated only by ~ 17 Å, a distance much shorter than the distance imposed by H-bonding. The most reasonable possibility is that the external rings of two neighbor molecules overlap, which would explain their brighter appearance. Annealing to 150 °C makes this structure more regular, and helps to disentangle its geometric structure (Figure S3a). The lattice is rhombohedral (a = 17.8 Å, α = 80º). Figure S3b shows the result of a DFT calculation with a similar structure (a = 16.3 Å, α = 88º). All the molecules have the same orientation, with four of their arms placed side to side with respect to adjacent molecular species, presumably enhancing π-π interactions; whereas the remaining two arms are pointing face to face to adjacent arms, as illustrated in Figure S3b.

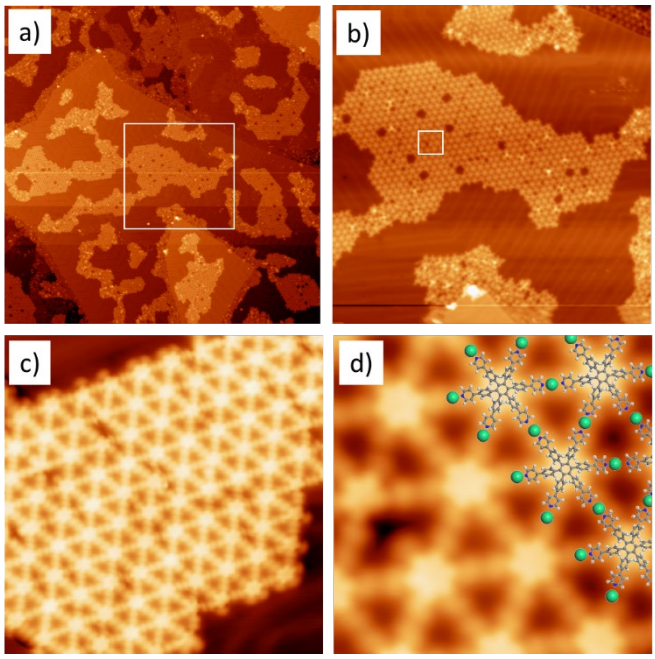

Figure 3: STM images of the Au(111) surface after depositing TTDP, Er and subsequent annealing to 200 ºC. Images (b) and (d) are close-up images of the areas marked with white squares in (a) and (b), respectively. Image (c) was taken on a different area. *a) 300 nm × 300 nm; 0.5 V, 0.1 nA; b) 100 nm × 100 nm; 0.5 V, 0.1 nA; c) 23 nm × 23 nm; 0.5 V, 0.02 nA; d) 7 nm × 7 nm; 0.5 V, 0.1 nA.*

After depositing Er onto this sample, with the substrate held at room temperature, there are still two different types of islands on the surface, but now their internal structure is much more disordered, with the Er atoms intercalated within the molecules (Figure S4).

Annealing to 200 °C transforms the molecular layer completely. Although there are some small irregular islands that appear at lower temperatures (Figure S5), most of the surface is covered by islands with an internal hexagonal arrangement (Figure 3). The TTDP molecules, with the main plane parallel to the surface, form an hexagonal structure with a lattice parameter of 23.4 ± 0.6 Å. This is much larger than in the hydrogen-bonded phase, but can be explained assuming the existence of an Er atom between every two molecules, forming -N-Er-N- bonds, and giving rise to a structure very similar to that shown in Figure 1c, where the Er atoms form a perfect kagome lattice. DFT calculations of a flat (exception for the rotation of the phenyl rings) free-standing layer with this structure gives an optimized lattice parameter of 25.24 Å, very close to the experimental results. Actually, the STM data are compatible with an epitaxial lattice described by the matrix

$$\begin{pmatrix} 10 & 5 \\ -5 & 5 \end{pmatrix},$$

which has a lattice parameter = 25.88 Å. DFT calculations (Figure S6) show that the adsorption geometry is very similar to the H-bonded phase. However, now the external rings are rotated a small angle also in the transversal direction. and since al the rings are rotated in the same direction, the molecular conformation is now chiral, giving the whole network a chiral texture (see below).

Figure 4 shows dI/dV spectra taken along the high symmetry directions in the lattice. Long range spectra (Figure 4a) show resonances at approximately 1.75 and 2.10 eV, and possible another one close to 2.60 eV. Once again, no strong resonance can be measured at negative voltages, except for the beginning of another one around -2.50 eV. However, getting closer to the surface (Figure 4b) reveals additional, more localized, electronic resonances at -0.55, -0.31, -0.14, 0.01 and 0.28 eV, all of them (except for the one centered at -0.14 eV), centered on the Er atom position. In addition, dI/dV maps (Figure S7) show the existence of other electronic states. It is worthy to note how the chirality predicted by DFT can be clearly appreciated in the 1.1-1.5 V dI/dV maps.

We have calculated the projected density of states on the metal organic layer (Figure S6b), but the abundance of Er *f* states and the artificial mixing with the gold states make its interpretation somewhat complicated. To simplify the system, and trying to elucidate the real electronic properties of a 2D lanthanide-kagome layer, we have also calculated an Er-TTDP free-standing layer. Figure 5a shows the optimized structure of such a layer. The lattice parameter is 25.24 Å, while the distance between Er atoms is 12.62 Å. Figure 5b shows an electronic isosurface (0.1 electrons/Å^3) colored according to the electrostatic potential at every point (going from red, more negative, to blue, more from positive). The Er atoms are positively charged (+ 0.5 |e$^-$|), while the N atoms hold a similar negative charge (- 0.5 |e$^-$|), which leaves the TTDP molecule with an absolute negative charge (- 1.5 |e$^-$|). Thus, the N-Er bond is mostly ionic, with almost no charge delocalization. This is further confirmed by the calculated band structure (Figure 5c), which consists mainly of flat bands along the Γ-K-M direction. These results agree with those reported for

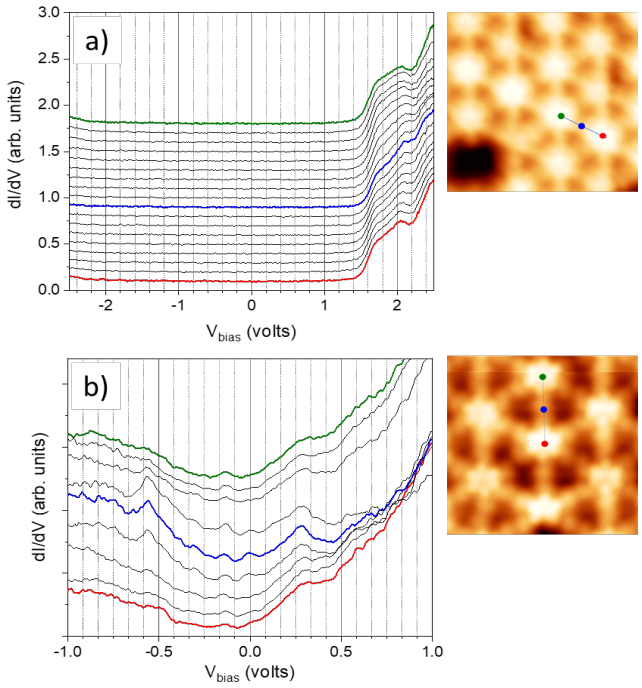

Figure 4: dI/dV spectra taken along the lines drawn in the corresponding STM images. *a) setpoint = 2.5 V, 0.5 nA; V_{rms} = 20 mV; b) setpoint = 1.0 V, 1.0 nA; V_{rms} = 30 mV.*

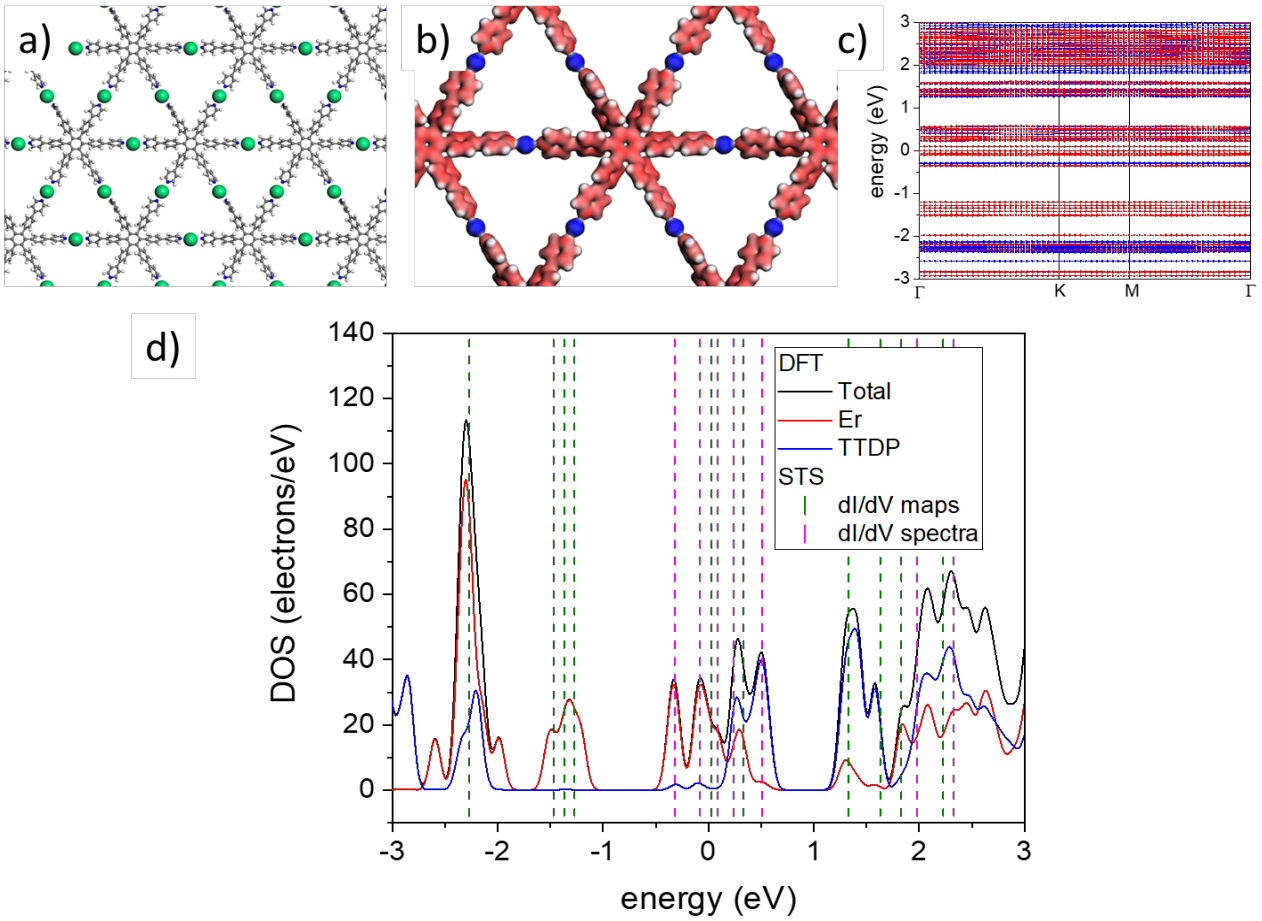

Figure 5: a) DFT calculated structure of an Er-TTDP free-standing layers. b) Close-up look at the same structure with an electron density isosurface (0.1 electrons/Å^3) colored according the electrostatic potential at every point. The color scale goes from red (more negative) to blue (more positive). c) Calculated band structure along the high symmetry directions of the reciprocal lattice. d) DFT calculated density of states (solid lines). The dashed vertical lines indicate the experimental energy position (shifted by 0.23 V to higher voltages) of the different resonances obtained from the STS spectra (green) and the dI/dV maps (magenta).

$Ln_{1.5}$HOTP (Ln = La, Nd), a 3D porous metal-organic framework composed of 2D $Ln_{1.5}$HOTP sheets stacked along the perpendicular direction, and where the Ln atoms form a kagome lattice within the sheets.[49,50] The DFT calculated density of states is plotted in Figure 5d (solid lines), while the experimental energy position of the different resonances obtained from the STS spectra (Figure 4) and the dI/dV maps (Figure S7) are indicated by dashed vertical lines (green and magenta, respectively). Note that the experimental data have been shifted by ~0.2 eV to higher voltages. Except for this shift, which is probably due to some transfer with the substrate, the agreement with the experimental data is quite good. (Note, however, that a full agreement is not to be expected due to the slightly different adsorption geometry). Also, according to the DFT calculations; the Er atoms hold a spin magnetic moment of ~ 2.2 μ_B.

Conclusion

In summary, deposition of Er atoms and TTDP molecules on a Au(111) substrate give rise, after annealing to 200 ºC, to a 2D, one monolayer thick, Er-TTDP metal-organic coordination network, where the molecules are arranged into a hexagonal lattice while the Er atoms form a perfect kagome lattice, with an electronic structure consisting mostly of flat bands. However, contrary to the flat bands appearing in kagome lattices containing 3d-metals, these flat bands do not arise due to the destructive interference of the electronic states,[51] rather to their localized character. On the other hand, the Er-TTDP MOCN does contain a kagome lattice of non-interacting Er atoms with a noticeably magnetic moment and connected through chiral linkers, which opens the way to the experimental study of the fascinating magnetic properties of real 2D kagome lattices composed of lanthanide elements, while at the same time extending to new materials the relatively new and then underexplored field of the exotic properties that systems combining a kagome lattice with a chiral structure may exhibit.[52]

Experimental Section

The scanning tunnelling microscopy (STM) experiments were performed in IMDEA Nanoscience in an ultra-high vacuum (UHV) setup with a base pressure of 1 × 10^{-10} mbar, hosting a commercial low-temperature STM from Omicron held at cryogenic temperatures (4.3 K, LakeShore). The images have been taken in constant current mode unless otherwise is stated, with a bias voltage applied to the sample, employing electrochemically etched Au tips. dI/dV curves and maps were measured using the lock-in technique (Stanford Research Systems SR830).

Prior to start the experiments, the Au(111) crystal (Mateck GmbH) was prepared by repeated cycles of standard Ar^+ sputtering (1.5 keV, 10 μA,

10 min, SPECS IQE 11/35) and subsequent annealing to 450 °C during 10 min.

TTDP molecules were deposited on top of the clean Au substrate, held at room temperature, by molecular beam epitaxy from a quartz crucible held at 350 ºC. To control the deposition, molecular flux was monitored by means of a quartz crystal microbalance (LewVac). Er atoms were deposited by electron bombardment from previously degassed rods (EFM3Ts evaporator) on top of the Au crystal held at room temperature and previously covered by less than one monolayer of TTDP species to have enough space for the metal-organic phase to be expressed.

DFT calculations were carried out using the DMol3 package[53,54] integrated in the Material Studio program of Dassault Systèmes. The electron exchange and correlation energies were treated with the generalized gradient approximation (GGA) of Perdew, Burke, and Ernzerhof.[55] The valence electron functions were expanded to a set of numerical atomic orbitals by a double-numerical basis with polarization functions (DNP), (a polarization d function on all the non-hydrogen atoms and a polarization p function on all the hydrogen atoms). DFT semicore pseudopotentials (DSPP),[56] which include some degree of relativistic effects, were used for Au and Er. The Tkatchenko and Scheffler (TS) scheme[57] for dispersion correction was also included. The convergence criteria, cutoff radius and Monkhorst-Pack K-point grid[58] are given in the Supplemental Information. Due to computational limitations, the metal surface was simulated by a repeated one-layer slab that was kept frozen, with a lateral supercell

$$\begin{pmatrix} 10 & 5 \\ -5 & 5 \end{pmatrix},$$

and a unit cell length in the perpendicular direction of 50 Å, in order to avoid the interaction between adjacent structures. Although the thickness of the gold layer can be considered small to study electronic effects, it is enough to induce an adsorption geometry in agreement with the experimental results.

Acknowledgements

This project has received funding from the Spanish Ministerio de Ciencia e Innovación (grant PID2022-136961NB-I00). We also acknowledge the support from the '(MAD2D-CM)-IMDEA-Nanociencia' and '(MAD2D-CM)-UCM' projects funded by Comunidad de Madrid, by the Recovery, Transformation and Resilience Plan, and by NextGenerationEU from the European Union. We thank funding from PERTE Chip project PDC2023-145871-I00.

Keywords: metal-organic networks • on surface synthesis • lanthanides • kagome lattice • STM

[1] I. Syozi, *Prog. Theor. Phys.* **1951**, *6*, 306–308.

[2] A. P. Ramirez, *Annual Review of Materials Science* **1994**, *24*, 453–480.

[3] J. Khatua, B. Sana, A. Zorko, M. Gomilšek, K. Sethupathi, M. S. R. Rao, M. Baenitz, B. Schmidt, P. Khuntia, *Phys Rep* **2023**, *1041*, 1–60.

[4] L. A. Fenner, A. A. Dee, A. S. Wills, *Journal of Physics: Condensed Matter* **2009**, *21*, 452202.

[5] S. H. Lee, H. Kikuchi, Y. Qiu, B. Lake, Q. Huang, K. Habicht, K. Kiefer, *Nat Mater* **2007**, *6*, 853–857.

[6] T. H. Han, J. S. Helton, S. Chu, D. G. Nocera, J. A. Rodriguez-Rivera, C. Broholm, Y. S. Lee, *Nature* **2012**, *492*, 406–410.

[7] E. Liu, Y. Sun, N. Kumar, L. Muechler, A. Sun, L. Jiao, S. Y. Yang, D. Liu, A. Liang, Q. Xu, J. Kroder, V. Süß, H. Borrmann, C. Shekhar, Z. Wang, C. Xi, W. Wang, W. Schnelle, S. Wirth, Y. Chen, S. T. B. Goennenwein, C. Felser, *Nat Phys* **2018**, *14*, 1125–1131.

[8] T. Kida, L. A. Fenner, A. A. Dee, I. Terasaki, M. Hagiwara, A. S. Wills, *Journal of Physics Condensed Matter* **2011**, *23*, 112205.

[9] G. Xu, B. Lian, S. C. Zhang, *Phys Rev Lett* **2015**, *115*, 186802.

[10] Q. Zhou, J. Wang, T. S. Chwee, G. Wu, X. Wang, Q. Ye, J. Xu, S. W. Yang, *Nanoscale* **2014**, *7*, 727–735.

[11] C. Barreteau, F. Ducastelle, T. Mallah, *Journal of Physics: Condensed Matter* **2017**, *29*, 465302.

[12] X. Zhang, Y. Zhou, B. Cui, M. Zhao, F. Liu, *Nano Lett* **2017**, *17*, 6166–6170.

[13] X. Huang, S. Zhang, L. Liu, L. Yu, G. Chen, W. Xu, D. Zhu, *Angewandte Chemie - International Edition* **2018**, *57*, 146–150.

[14] J. X. Yin, B. Lian, M. Z. Hasan, *Nature* **2022**, *612*, 647–657.

[15] Y. Wang, H. Wu, G. T. McCandless, J. Y. Chan, M. N. Ali, *Nature Reviews Physics* **2023**, *5*, 635–658.

[16] J. G. Checkelsky, B. A. Bernevig, P. Coleman, Q. Si, S. Paschen, *Nat Rev Mater* **2024**, *9*, 509–526.

[17] R. L. Johnston, R. Hoffmann, *Z Anorg Allg Chem* **1992**, *616*, 105–120.

[18] H. Ishikawa, T. Okubo, Y. Okamoto, Z. Hiroi, *J Physical Soc Japan* **2014**, *83*, DOI 10.7566/JPSJ.83.043703.

[19] T. Kambe, R. Sakamoto, K. Hoshiko, K. Takada, M. Miyachi, J. H. Ryu, S. Sasaki, J. Kim, K. Nakazato, M. Takata, H.

Nishihara, *J Am Chem Soc* **2013**, *135*, 2462–2465.
[20] J. Cui, Z. Xu, *Chemical Communications* **2014**, *50*, 3986–3988.
[21] D. Sheberla, L. Sun, M. A. Blood-Forsythe, S. Er, C. R. Wade, C. K. Brozek, A. Aspuru-Guzik, M. Dincă, *J Am Chem Soc* **2014**, *136*, 8859–8862.
[22] N. Xu, W. Shi, D. Z. Liao, S. P. Yan, P. Cheng, *Inorg Chem* **2008**, *47*, 8748–8756.
[23] Z. L. Dun, J. Trinh, K. Li, M. Lee, K. W. Chen, R. Baumbach, Y. F. Hu, Y. X. Wang, E. S. Choi, B. S. Shastry, A. P. Ramirez, H. D. Zhou, *Phys Rev Lett* **2016**, *116*, 157201.
[24] G. Venturini, B. C. El Idrissi, B. Malaman, *J Magn Magn Mater* **1991**, *94*, 35–42.
[25] J. X. Yin, W. Ma, T. A. Cochran, X. Xu, S. S. Zhang, H. J. Tien, N. Shumiya, G. Cheng, K. Jiang, B. Lian, Z. Song, G. Chang, I. Belopolski, D. Multer, M. Litskevich, Z. J. Cheng, X. P. Yang, B. Swidler, H. Zhou, H. Lin, T. Neupert, Z. Wang, N. Yao, T. R. Chang, S. Jia, M. Zahid Hasan, *Nature* **2020**, *583*, 533–536.
[26] W. Ma, X. Xu, J. X. Yin, H. Yang, H. Zhou, Z. J. Cheng, Y. Huang, Z. Qu, F. Wang, M. Z. Hasan, S. Jia, *Phys Rev Lett* **2021**, *126*, 246602.
[27] S. Furukawa, H. Uji-I, K. Tahara, T. Ichikawa, M. Sonoda, F. C. De Schryver, Y. Tobe, S. De Feyter, *J Am Chem Soc* **2006**, *128*, 3502–3503.
[28] U. Schlickum, R. Decker, F. Klappenberger, G. Zoppellaro, S. Klyatskaya, W. Auwärter, S. Neppl, K. Kern, H. Brune, M. Ruben, J. V. Barth, *J Am Chem Soc* **2008**, *130*, 11778–11782.
[29] J. Tu, W. Song, B. Chen, Y. Li, L. Chen, *Chemistry – A European Journal* **2023**, *29*, e202302380.
[30] G. Pawin, K. L. Wong, D. Kim, D. Sun, L. Bartels, S. Hong, T. S. Rahman, R. Carp, M. Marsella, *Angewandte Chemie International Edition* **2008**, *47*, 8442–8445.
[31] Z. Shi, N. Lin, *J Am Chem Soc* **2009**, *131*, 5376–5377.
[32] L. Dong, Z. A. Gao, N. Lin, *Prog Surf Sci* **2016**, *91*, 101–135.
[33] Y. fang Geng, P. Li, J. zhen Li, X. mei Zhang, Q. dao Zeng, C. Wang, *Coord Chem Rev* **2017**, *337*, 145–177.
[34] J. Liu, N. Lin, *Chempluschem* **2023**, *88*, e202200359.
[35] J. Rodríguez-Fernández, K. Lauwaet, M. Á. Herranz, N. Martín, J. M. Gallego, R. Miranda, R. Otero, *Journal of Chemical Physics* **2015**, *142*, DOI 10.1063/1.4913326.
[36] D. Kumar, J. Hellerstedt, B. Field, B. Lowe, Y. Yin, N. V. Medhekar, A. Schiffrin, *Adv Funct Mater* **2021**, 2106474.
[37] G. Galeotti, F. De Marchi, E. Hamzehpoor, O. MacLean, M. Rajeswara Rao, Y. Chen, L. V. Besteiro, D. Dettmann, L. Ferrari, F. Frezza, P. M. Sheverdyaeva, R. Liu, A. K. Kundu, P. Moras, M. Ebrahimi, M. C. Gallagher, F. Rosei, D. F. Perepichka, G. Contini, *Nat Mater* **2020**, *19*, 874–880.
[38] L. Yan, O. J. Silveira, B. Alldritt, O. Krejčí, A. S. Foster, P. Liljeroth, *Adv Funct Mater* **2021**, *31*, 2100519.
[39] Z. Gao, C. H. Hsu, J. Liu, F. C. Chuang, R. Zhang, B. Xia, H. Xu, L. Huang, Q. Jin, P. N. Liu, N. Lin, *Nanoscale* **2019**, *11*, 878–881.
[40] A. Kumar, K. Banerjee, A. S. Foster, P. Liljeroth, *Nano Lett* **2018**, *18*, 5596–5602.
[41] L. Yan, I. Pohjavirta, B. Alldritt, P. Liljeroth, L. Yan, I. Pohjavirta, B. Alldritt, P. Liljeroth, *ChemPhysChem* **2019**, *20*, 2297–2300.
[42] D. Écija, J. I. Urgel, A. P. Seitsonen, W. Auwärter, J. V. Barth, *Acc Chem Res* **2018**, *51*, 365–375.
[43] S. O. Parreiras, J. M. Gallego, D. Écija, *Chemical Communications* **2023**, *59*, 8878–8893.
[44] D. Moreno, B. Cirera, S. O. Parreiras, J. I. Urgel, N. Giménez-Agulló, K. Lauwaet, J. M. Gallego, J. R. Galán-Mascarós, J. I. Martínez, P. Ballester, R. Miranda, D. Écija, *Chemical Communications* **2021**, *57*, 1380–1383.
[45] S. O. Parreiras, D. Moreno, B. Cirera, M. A. Valbuena, J. I. Urgel, M. Paradinas, M. Panighel, F. Ajejas, M. A. Niño, J. M. Gallego, M. Valvidares, P. Gargiani, W. Kuch, J. I. Martínez, A. Mugarza, J.

Camarero, R. Miranda, P. Perna, D. Écija, *Small* **2021**, *17*, 2102753.
[46] D. Moreno Cerrada, J. Santos, S. O. Parreiras, C. Martín-Fuentes, K. Lauwaet, J. I. Urgel, R. Miranda, N. Martín, J. M. Gallego, D. Ecija, D. Moreno, D. Écija, D. Moreno, S. O. Parreiras, C. Martín-Fuentes, K. Lauwaet, J. I. Urgel, R. Miranda, N. Martín, D. Écija, J. Santos, J. M. Gallego, *Chemistry – A European Journal* **2023**, e202300461.
[47] D. Moreno, S. O. Parreiras, J. I. Urgel, B. Muñiz-Cano, C. Martín-Fuentes, K. Lauwaet, M. Valvidares, M. A. Valbuena, J. M. Gallego, J. I. Martínez, P. Gargiani, J. Camarero, R. Miranda, D. Écija, *Small* **2022**, *18*, 2107073.
[48] S. O. Parreiras, D. Moreno, S. K. Mathialagan, B. Muñiz-Cano, C. Martín-Fuentes, M. Tenorio, L. Černa, J. I. Urgel, K. Lauwaet, M. Valvidares, M. A. Valbuena, J. M. Gallego, J. I. Martínez, P. Gargiani, R. Miranda, J. Camarero, D. Écija, *Nanoscale* **2023**, *15*, 7267–7271.
[49] G. Skorupskii, B. A. Trump, T. W. Kasel, C. M. Brown, C. H. Hendon, M. Dincă, *Nature Chemistry 2019 12:2* **2019**, *12*, 131–136.
[50] G. Skorupskii, K. N. Le, D. L. M. Cordova, L. Yang, T. Chen, C. H. Hendon, M. Q. Arguilla, M. Dincă, *Proc Natl Acad Sci U S A* **2022**, *119*, e2205127119.
[51] D. Gerlach, J. Noack, K. Bischof, J. López De Andrés, M. Ruiz-Toranzo, C. Antich, L. Zheng, L. Feng, W. Yong-Shi, *Chinese Physics B* **2014**, *23*, 077308.
[52] X. Li, D. Wang, H. Hu, Y. Pan, *Nanotechnology* **2024**, *35*, 145601.
[53] B. Delley, *J Chem Phys* **1998**, *92*, 508.
[54] B. Delley, *J Chem Phys* **2000**, *113*, 7756.
[55] J. P. Perdew, K. Burke, M. Ernzerhof, *Phys Rev Lett* **1996**, *77*, 3865–3868.
[56] B. Delley, *Phys Rev B* **2002**, *66*, 155125.
[57] A. Tkatchenko, M. Scheffler, *Phys Rev Lett* **2009**, *102*, 073005.
[58] H. J. Monkhorst, J. D. Pack, *Phys Rev B* **1976**, *13*, 5188–5192.

Entry for the Table of Contents

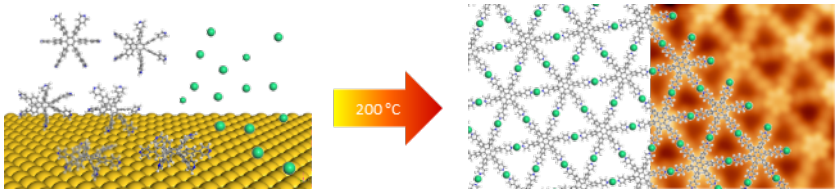

The deposition and posterior annealing of TTDP molecules and Er atoms on a Au(111) surface allows the creation of a perfect kagome lattice of lanthanide elements.